Electronic Supplementary Material (ESI) for Chemical Science.

Electronic Supplementary Information

The proton conduction mechanism in a material consisting of packed acids

Authors: Takaya Ogawa, Takashi Aonuma, Takanori Tamaki, Hidenori Ohashi, Hiroshi Ushiyama, Koichi Yamashita, Takeo Yamaguchi

Contents

I. Synthesis procedures for the experimental section
II. Characterization of the materials
III. Detailed information about the experimental measurements
IV. Detailed information about the calculations
V. Conceptual images of the ZrSPP-SPES interfaces
VI. The effect of the packed-acid mechanism on hopping
VII. The origin of the high wavenumber bands in the FT-IR spectra
VIII. Concerted hopping during AIMD
IX. A suitable density of sulfonic acids (λ) for the packed-acid mechanism
X. References

I. Synthesis procedures for the experimental section

Synthesis of capping-ZrSPP–SPES.

Sulfonated poly(arylene ether sulfone) (SPES), metasulfophenylphosphonic acid (SPPA), and APS–Zr were synthesized as follows. The mole fraction of the sulfonated unit in SPES was 0.48. The weight-averaged molecular weight (M_w) of SPES was 166,000, and the polydispersity index (M_w/M_n) was 2.99. Capping was performed via the dropwise addition of a 10 wt% solution of SPES in *N*-methyl-2-pyrrolidone (NMP) to a 10 wt% solution of APS–Zr in NMP. The weight ratio of the precursor to SPES was 1:1. The mixed solution was cast onto a glass plate and dried at 60 °C overnight and then dried at 110 °C for more than 6 h under vacuum. APS–Zr was converted to ZrSPP in the membrane by treating the membrane with a solution of SPPA in 1.5 M H_2SO_4 at 100 °C for 18 h[S1]. Any excess acid was completely washed away by stirring for 24 h in methanol and water with several exchanges of the cleaning solution (see Table S1).

Synthesis ofsimple-mixing-ZrSPP-SPES.

Simple-mixing-ZrSPP–SPES was synthesized by modifying previously reported procedures[S2,S3]. First, ZrSPP was prepared according to the method described in Ref.S1. ZrSPP was initially dissolved in water using ultrasonic waves for 20 min, followed by the addition of NMP. This solution was treated with ultrasonication for 20 min. The water in the solution was evaporated at 80 °C, and a 5 wt% solution of ZrSPP in NMP was prepared. The ZrSPP solution was added dropwise to a 20 wt% SPES solution in NMP with stirring, and a transparent solution of ZrSPP–SPES was obtained. The solution was then cast onto a glass plate and heated at 60 °C overnight. Next, the sample was dried under vacuum at 100 °C for 12 h. The electrolyte was then washed with methanol, stirred for 4 h, and dried under vacuum at 100 °C for 1 h.

Synthesis of APS–Zr[S4]

Materials

Anhydrous isopropylalcohol (IPA), acetylacetone (AcAc), 3-aminopropyl-methyl diethoxysilane (APS), 85% zirconium(IV) butoxide in *n*-butanol solution, 1 M nitric acid, and NMP were purchased from Wako Chemical Co., Ltd. and used as received.

Procedures

Zirconium(IV) oxide with AcAc and APS (APS–Zr) as surface modifiers was synthesized using a sol–gel method. AcAc was used to control the hydrolysis and condensation of zirconium(IV) butoxide in IPA and to disperse the zirconium(IV) oxide in polar organic solvents such as NMP. The aminosilane coupling agent, APS, which was used for the functionalization of the surface of zirconium(IV) oxide, was applied to stabilize the nanocomposite composed of ZrO_2 and SPES in solution through electrostatic interactions between the amino and sulfonic acid groups. Zirconium(IV) butoxide solution (5.65 g) and 2.50 g of AcAc were mixed in 200 mL of anhydrous IPA for 2.5 h in a glove box. Then, 1.75 g of APS was added to the mixture and stirred for 30 min. Subsequently, 5 mL of 1 M nitric acid was added dropwise, and the solution was stirred overnight. Finally, the APS–Zr powder was obtained after drying at 80 °C for 6 h. The mole ratio of Zr, AcAc, and APS was fixed at 1:2:0.75.

Synthesis of SPPA[S1]

Materials

Phenylphosphonic acid (purity greater than 98%) and SO_3(60%) were purchased from Aldrich and Wako Pure Chemical Industries, Ltd, respectively.

Procedures

Metasulfophenylphosphonic acid ($H_2O_3PC_6H_4SO_3H$, SPPA) was synthesized by the direct reaction of phenylphosphonic acid with SO_3 at 180 °C for 24 h. The mole ratio of phenylphosphonic acid to SO_3 was fixed at 4:1. The reaction was terminated by pouring distilled water into the resultant viscous liquid, and an SPPA solution in 1.5 M H_2SO_4 was obtained.

The synthesis of SPES[S5]

Materials

4,4′-Dichlorodiphenylsulfone (DCDPS) was purchased from Tokyo Chemical Industry Co., Ltd., recrystallized from toluene, and dried *in vacuo*. 4,4′-Biphenol (BP), purchased from Tokyo Chemical Industry Co., Ltd., and potassium carbonate, purchased from Wako Chemical Co., Ltd., were dried *in vacuo* before use. Anhydrous NMP, anhydrous toluene, and sulfuric acid were purchased from Wako Chemical Co., Ltd. and used as received. 3,3′-Disulfonated-4,4′-dichlorodiphenyl sulfone monomer (DSDCDPS) was synthesized from 4,4′-dichlorodiphenyl sulfone and fuming sulfuric acid (30% SO_3, Wako Chemical Co., Ltd.) according to a previously reported method. The synthesis of the DSDCDPS monomer was confirmed by ^{1}H-NMR and FT–IR measurements.

Procedures

The materials used in the synthesis of SPES (DCDPS, DSDCDPS, BP, and potassium carbonate) were dried overnight at a temperature greater than 100 °C *in vacuo* before the synthesis to remove any residual water. The synthesis reaction of SPES is a nucleophilic aromatic substitution polycondensation and was conducted according to the previously reported method. The degree of sulfonation, 0.48, was determined as the mole fraction (DSDCDPS/(DSDCDPS + DCDPS)) and controlled by adjusting the ratio of DSDCDPS monomer to DCDPS monomer, 1:1.

II. Characterization of the materials

TEM images of APS–Zr–SPES and capping-ZrSPP–SPES are shown in Fig. S1a-d. In Fig. S1, the dark regions are ZrSPP or APS–Zr, and the grey regions are SPES. Figures S1a and S1b demonstrate that APS–Zr forms a homogeneous and fine dispersion on the nanoscale. This dispersion generates a ZrSPP–SPES interface. As indicated in Fig. S1c and d, ZrSPP also forms a fine dispersion even on the nanoscale. By contrast, the scanning electron microscope (SEM) images of the simple-mixing-ZrSPP–SPES interface (Fig. S1e and f) show that the ZrSPP particles in the simple-mixing-ZrSPP–SPES sample are much larger (approximately 3 μm). The surface area of the ZrSPP–SPES interface is greater in capping-ZrSPP–SPES than in simple-mixing-ZrSPP–SPES. Thus, the simple-mixing method described in section I can disperse various inorganic particles into several electrolytes (Refs. S2, S3), but it is difficult to generate this interface with this combination of ZrSPP–SPES. As mentioned in the discussion of the high O–S–O wavenumber (section VII in SI), the capping method appears to be critical for the creation of the interface.

TEM images of APS–Zr–SPES and capping-ZrSPP–SPES were acquired by the Toray Research Centre, Inc., and SEM analysis was performed by the Centre for Advanced Materials Analysis at the Tokyo Institute of Technology.

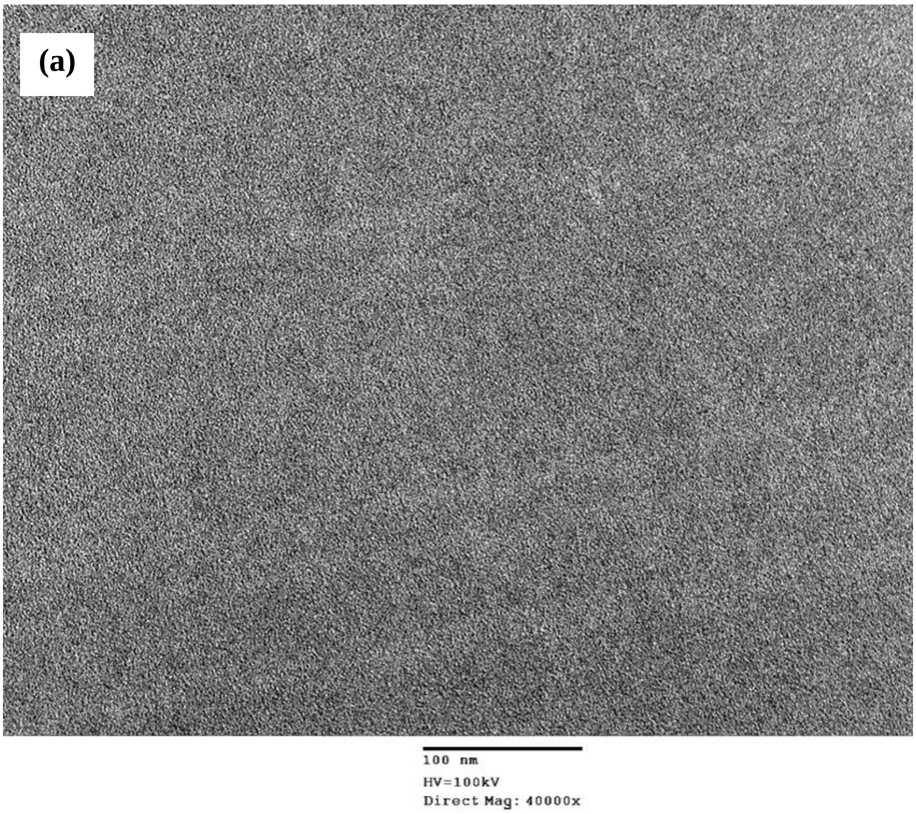
(a)
100 nm
HV=100kV
Direct Mag: 40000x

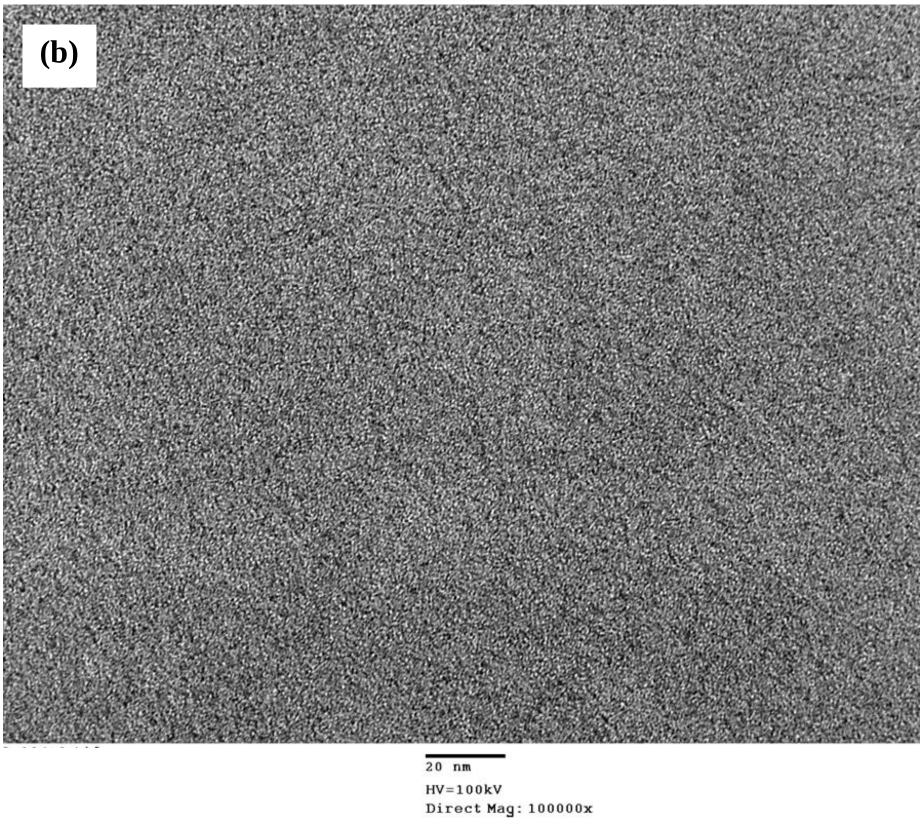
(b)
20 nm
HV=100kV
Direct Mag: 100000x

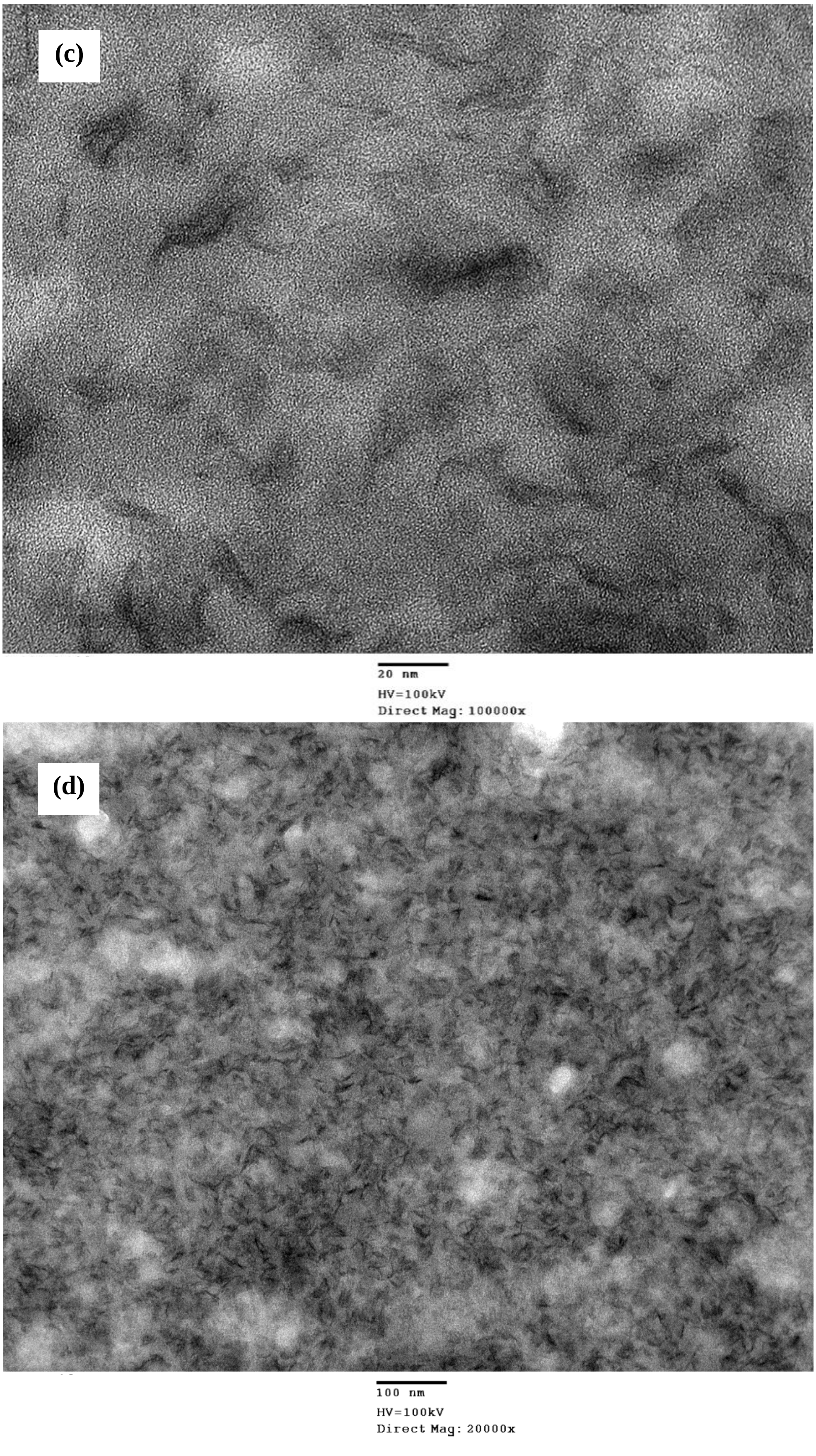
(c)
20 nm
HV=100kV
Direct Mag: 100000x
(d)
100 nm
HV=100kV
Direct Mag: 20000x

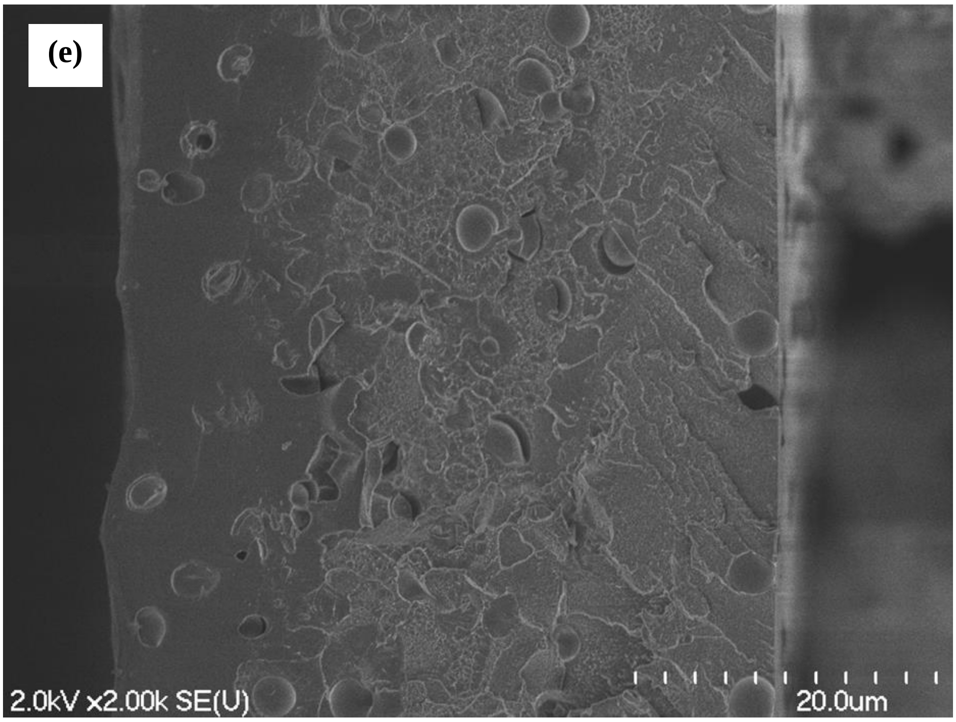

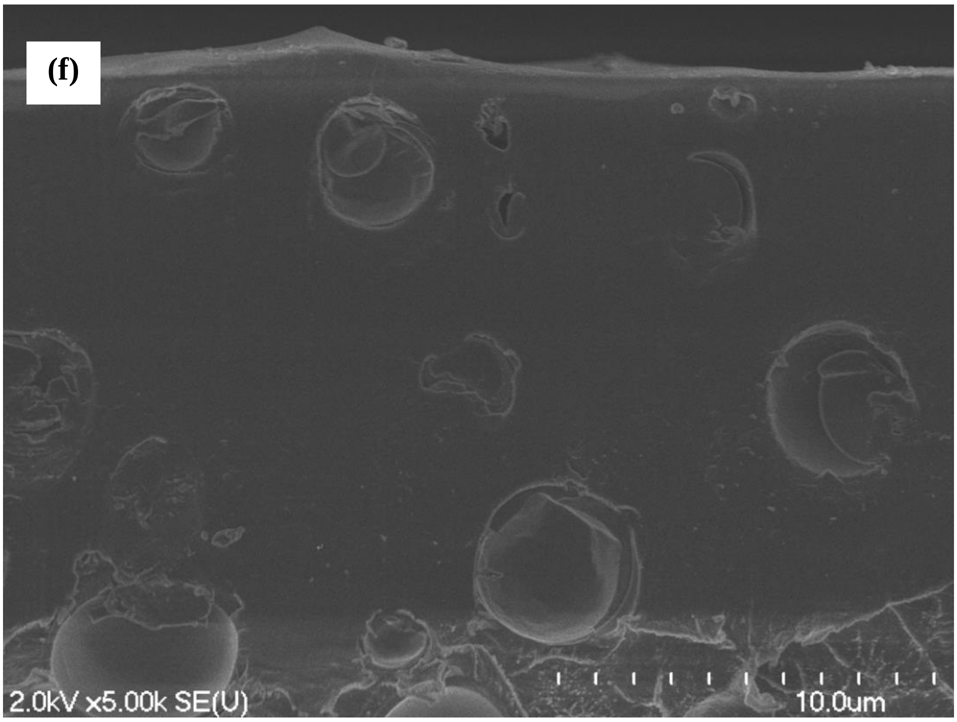

Figure S1. TEM images of (a), (b) APS–Zr–SPES and (c) (d) capping-ZrSPP–SPES and (e), (f) SEM images of simple-mixing-ZrSPP–SPES.

Full FT–IR spectra of APS–Zr, ZrSPP, SPES, capping-ZrSPP–SPES, and simple-mixing-ZrSPP–SPES are shown in Fig. S2. The conversion of APS–Zr to ZrSPP in the capping-ZrSPP–SPES samples was confirmed by the peaks at approximately 1260 and 610 cm^{-1} due to PO_3; 968 cm^{-1} due to P–O; and 600–700, 1000–1075, and 1150–1250 cm^{-1} due to SO_3H[S1,S5]. Removal of APS in the capping-ZrSPP–SPES samples was confirmed by the diminished peak arising from the methyl group in APS at approximately 3000 cm^{-1} (Ref. S4).

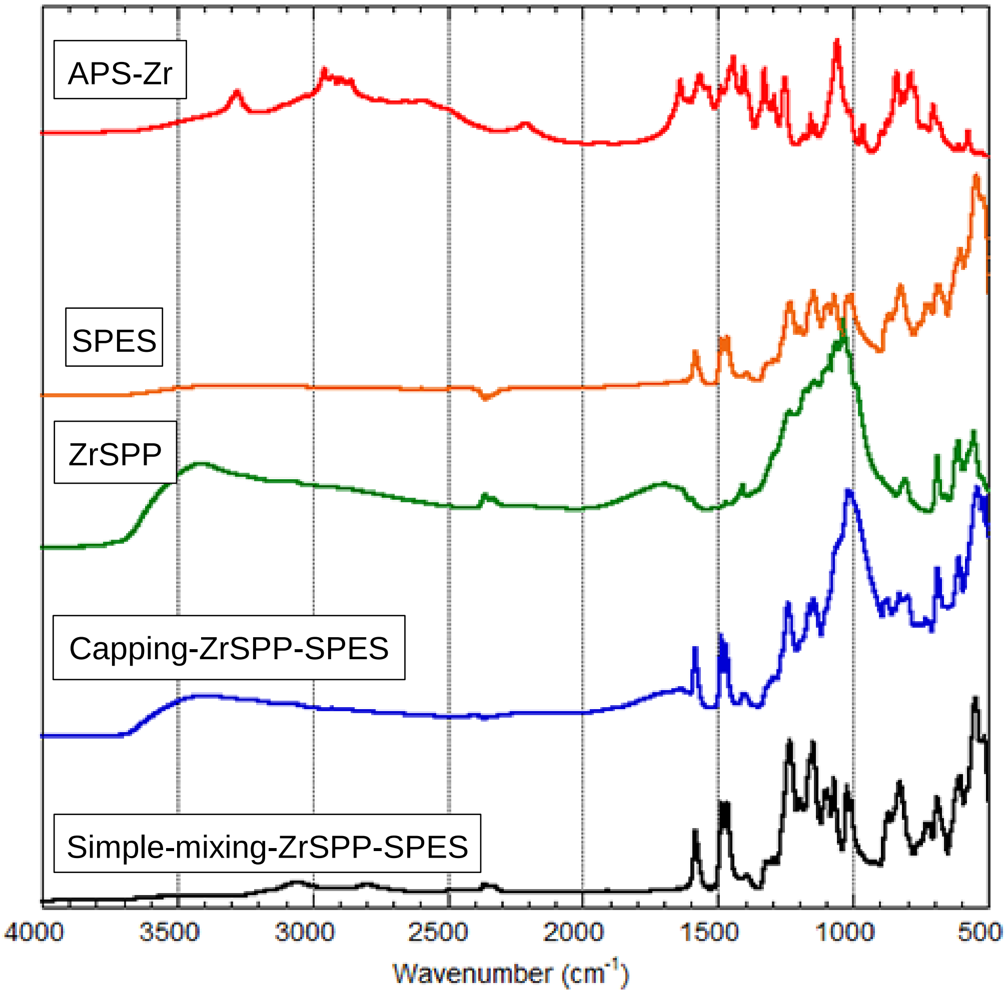

Figure S2. FT–IR spectra of each material.

The ICP–AES results for the capping-ZrSPP–SPES samples were measured by dissolving the material in NMP. The capping-ZrSPP–SPES sample did not completely dissolve, which means that the absolute value is not valid. However, the ratio of Zr:P was almost 1:2, and no Si was detected (Table S1). Thus, the Si from the APS and SPPA was removed.

Table S1. ICP–AES results for the capping-ZrSPP–SPES sample.

	Zr	S	P	Si
(mol/L)	0.04	0.56	0.09	0.00

III. Detailed information on the experimental analysis

The characterizations in the present report were performed using the following equipment. Dynamic light scattering was performed with a Zetasizer Nano S90 (Malvern Instruments Ltd.) equipped with a 4-mW He–Ne laser, FT–IR spectra were measured with an FT–IR-6200 (Jasco Co., Ltd.) spectrophotometer in attenuated total reflection mode. Proton conductivities were determined using a two-probe AC impedance method with a Solatron 1260 impedance analyzer in the frequency range of 1000 Hz to 1 MHz and at a signal amplitude of 50 mV, and the resistance was read from the crossing point of the Re *Z* axis (Fig. S3). When the Cole–Cole plot did not have a crossing point with the Re *Z* axis, we read the nearest point to the Re *Z* axis, which guaranteed that the conductivity of the electrolyte was at least this large. The proton conductivity was calculated using the following equation:

$$\sigma = \frac{d}{RA},$$

where R, d, and A are the resistance, distance to the electrode, and area of electrolyte that conducts protons, respectively. The relative humidity (RH) was controlled by a forced convection-type temperature and humidity chamber (SH-241, Espec Co., Ltd.).

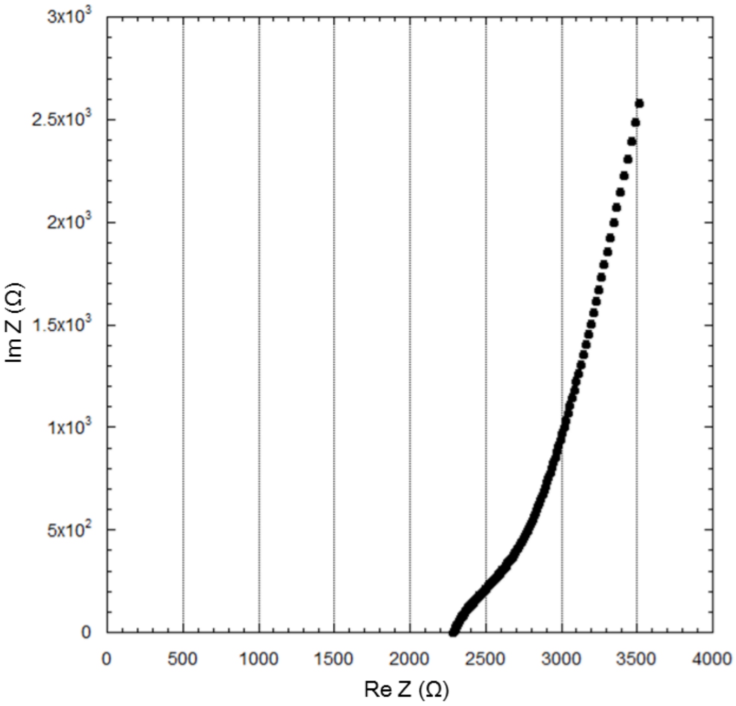

Figure S3. Typical Cole–Cole plot for capping-ZrSPP–SPES. The Cole–Cole plot was obtained at 90 °C and 50% RH.

The activation energies (E_a) for proton conductivity were calculated from the following equations based on the Nernst–Einstein equation and Arrhenius plot of diffusivity:

$$\sigma = \frac{D_T c e^2}{k_\mathrm{B} T} = \frac{A}{T} \exp\left(-\frac{E_a}{RT}\right)$$

$$D_T = D_0 \exp\left(-\frac{E_a}{RT}\right)$$

where T, R, c, e, k_B, D_T, D_0, and A are the absolute temperature, gas constant, proton concentration , electron charge, Boltzmann constant, temperature-dependent diffusivity coefficient, reference diffusivity coefficient, and pre-exponential factor, respectively[46]. This equation assumes that diffusivity does not depend on the proton concentration, and that the proton concentration does not depend on the temperature. In general, the E_a for proton conductivity is experimentally calculated from an Arrhenius plot[49,S6,S19]. In the case of calculating E_a from Arrhenius plots at 80, 60, and 40% RH (60–90 °C), the values of E_a were 10, 13, and 20 kJ/mol in capping-ZrSPP–SPES, and 14, 16, and 25 kJ/mol in SPES, respectively. In this research, the experimental E_a was quantitatively compared with the E_a obtained by *ab initio* calculations. The appropriate E_a should be calculated using the Nernst–Einstein equation in this case.

IV. Detailed information on the calculations

For the theoretical analysis, we performed density functional theory (DFT) calculations using the RPBE (Revised Perdew–Burke–Ernzerhof) functional[38]. We used single Kleinman–Bylander projectors to represent each angular momentum channel[S8] and a relativistic polarized calculation to estimate the effect of spin. A double-zeta split-valence basis set with polarization orbitals was used[39]. Norm-conserving pseudopotentials were applied using the improved Troullier–Martins method with nonlinear core corrections[S9]. All calculations were performed using the SIESTA (Spanish Initiative for Electronic Simulations with Thousands of Atoms) 2.0.1 software package[37].

The base layer structure of the ZrSPP model was based on the nearly identical structure of zirconium phosphate (ZrP)[S10]. The hydroxyl group (–OH) was replaced by BS to describe ZrSPP according to Alberti *et al*[S6]. The lattice constant of a unit cell—including the vacuum layer—was nearly monoclinic: (a, b, c, α, β, γ) = (9.6 Å, 5.8 Å, 133.3 Å, 88.9°, 100.5°, 88.8°). The vacuum region was assumed to be approximately 100 Å in the c direction. One layer of the ZrSPP unit cell was duplicated in the plane direction using a periodic boundary condition with $2 \times 2 \times 1$ k-grid sampling. To reduce the calculation cost, the interface side of the ZrSPP contained the BS, and the non-interface side contained the OH. We confirmed that these approximations produced negligible differences. The positions of the atoms on the non-interface side were fixed.

In the procedures for constructing the models, the water molecules were allocated on the ZrSPP surface at a reasonable distance spacing without any arbitrariness. After allocating the water molecules, benzene sulphonic acid was placed on the water layer at a reasonable distance spacing. After these allocations, the models were optimized with the termination condition that the maximum tolerance force was 0.01 eV/Å. Forty-two patterns of ZrSPP–BS interface models including the water molecules were studied. We confirmed that the acid and water constructed an H-bonding network and that the average number of H-bonds generated by each water molecule was 3.37.

The E_a values for hopping and reorientation and the $P_{<2.6}$ value for the *Roo* in each of the classified groups (Fig. 9a, b) at the above interfaces were examined. We use the forty-two patterns of ZrSPP–BS interface models including the water molecules as initial structure (reactants). From each reactant geometry, we moved one of the protons of any one of the water molecules or SO_3H to the oxygen atoms in water or SO_3H along H-bond in case of hopping, or other direction of H-bond in case of reorientation. And then, the geometry was optimized while fixing the positions of the moved proton and the proton-donating and/or -accepting oxygen atoms. Finally, all of the atoms were optimized, and the final states (products) were obtained. To find the transition states and minimum energy paths that connect the reactant and the product, we applied the nudged elastic band method to find E_a[41–43]. The averaged *Roo* for each step in which the hopping and reorientation occurred in concert is shown in Fig. 8. The structures in the figures were visualized using VESTA (Visualization for Electronic and STructural Analysis)[S11].

An H-bond was defined as follows: bond angle > 110° according to IUPAC[S12] and *Roo*> 2.4 Å but < 3.5 Å. The minimum *Roo* value found in these simulations was 2.4 Å. The experimental distribution function indicates that the first shell of water exists with an upper limit of 3.5 Å[S13]. Therefore, we set the maximum *Roo* value to 3.5 Å. We assumed that one proton can belong to only one H-bond. If one proton had two possible candidates, we assigned the proton to the H-bond with the shorter *Roo* value. This definition was utilized to determine the number of H-bonds in each water molecule and excluded distant water molecules when calculating the exact $P_{<2.6}$ value.

$P_{<2.6}$ was calculated based on the number of H-bonds as follows:

$$P_{<2.6} = \frac{(<2.6)}{(\text{Total})},$$

in which "< 2.6" and "Total" represent the number of H-bonds whose *Roo* values are < 2.6 Å in each classified group (Fig. 9a, b) and the total number of H-bonds in each group, respectively. Each value is provided in Table S2.

Table S2 shows the detailed numbers that accompany Table 1.

Using the above calculation methods and models, AIMD was performed to confirm the proposed proton behavior, *i.e.*, the "packed-acid mechanism". A Nosé thermostat[46] was utilized to maintain the system temperature to 363 K. A time step of 0.2 fs was used, and 16 patterns of AIMD were operated for almost 10 ps from the initial optimized structures with 1-5 water molecules per SO_3H. During AIMD, the structure of the ZrSPP base layer was replaced with a hydrogen atom to reduce the calculation costs. The positions of these hydrogen atoms were fixed. In addition, the hydrogen atom of para-BS was fixed by assuming that BS was attached to a solid material such as SPES.

Table S2. The number of H-bonds in each group. "< 2.6" and "Total" indicate the number of H-bonds with *Roo*< 2.6 Å and the total number of H-bonds, respectively. The total number of H-bonds in the H3 group is low because few H-bonds exist between H_3O^+ and SO_3H in our 42 patterns of the interface model. Thus, H_3O^+ does not bind with SO_3H. Therefore, the same conclusion can be derived for the low $P_{<2.6}$ value of H3.

Group	Subgroup	Component	< 2.6	Total
From H_2O	W1	$H_2O \rightarrow H_2O$	66	389
	W2	$H_2O \rightarrow SO_3^-$	7	118
	W3	$H_2O \rightarrow SO_3H$	1	56
From H_3O^+	H1	$H_3O^+ \rightarrow H_2O$	66	76
	H2	$H_3O^+ \rightarrow SO_3^-$	21	34
	H3	$H_3O^+ \rightarrow SO_3H$	0	2
From SO_3H	S1	$SO_3H \rightarrow H_2O$	20	27
	S2	$SO_3H \rightarrow SO_3^-$	6	9
	S3	$SO_3H \rightarrow SO_3H$	0	18

V. Conceptual images of the ZrSPP-SPES interfaces

The contents of section V and VI explain the contents in section VII and VIII in advance. In this section, we present conceptual images of the simple-mixing-ZrSPP–SPES and capping-ZrSPP–SPES interfaces in Figs. S4a and b, respectively. In an individual proton-donor region, which the simple-mixing-ZrSPP–SPES is assumed to be, water molecules are attracted to the proton donors SO_3H and H_3O^+. These bound water molecules can attract other water molecules[S13] and form $H_5O_2^+$ and $H_9O_4^+$. The general proton-conduction mechanism conducts a proton via structural diffusion. However, proton has a highly attractive interaction, and a rigid H-bond network is constructed around the proton donor. Thus, reorientation, the rate-determining step, does not occur around the proton donor, *i.e.*, the inactive region (Fig. S4a). In contrast to the inactive region, in a packed-acid structure such as the capping-ZrSPP–SPES interface, proton donors can interact with each other. Acid–acid interactions weaken the H-bonds, such as $H_3O^+ \rightarrow SO_3H$ (H3) and $SO_3H \rightarrow SO_3H$ (S3), because of the low proton affinity of the proton donors due to the interaction (Fig. S4b). A weak H-bond network leads to a flexible H-bond network and facilitates reorientation. The packed-acid mechanism occurs in a packed-acid structure with acid–acid interaction.

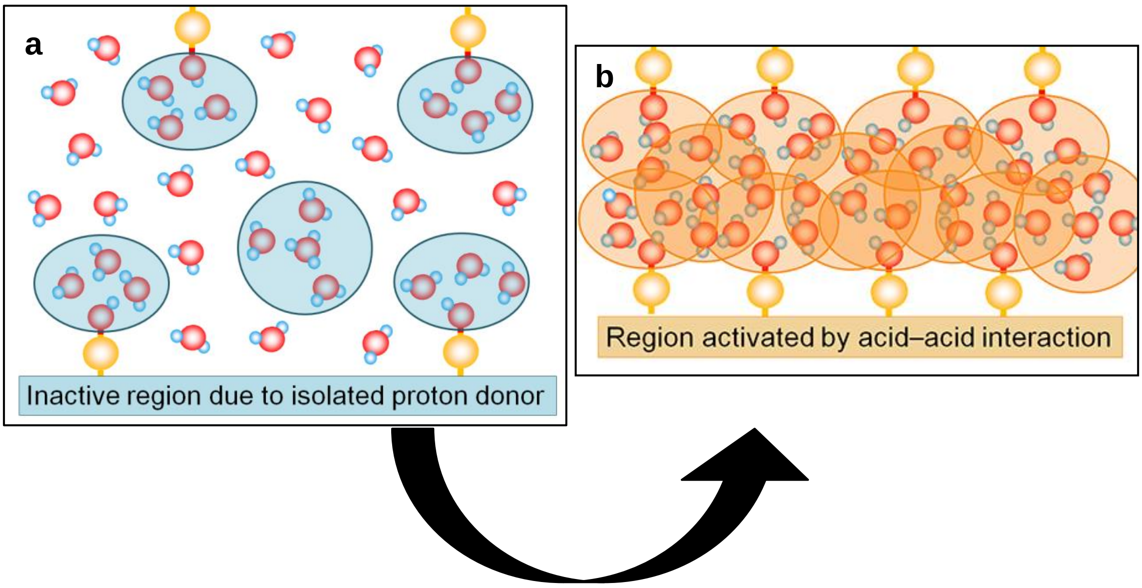

Figure S4. Conceptual images of (a) an individual acid region isolated from other acids and (b) a packed acid structure. (**a**) and (**b**) are the images of simple-mixing-ZrSPP–SPES and capping-ZrSPP–SPES, respectively.

VI. The effect of the packed-acid mechanism on hopping

As shown in Fig. S5, the value of *Roo* between water and SO_3H is closely related to the number of sequential SO_3H molecules. We determined that *Roo* becomes shorter as the number of sequential SO_3H molecules that combine with SO_3H bound to water increases. Because these H-bond networks preferentially form in a packed-acid structure, hopping and reorientation are facilitated. Based on the data in Fig. 8a, the E_a value for hopping is reduced by 2.81 kJ/mol when *Roo* is shortened by 0.01 Å. The absolute value is not precise but indicates that this contraction of *Roo* between SO_3H and water has a substantial impact on E_a.

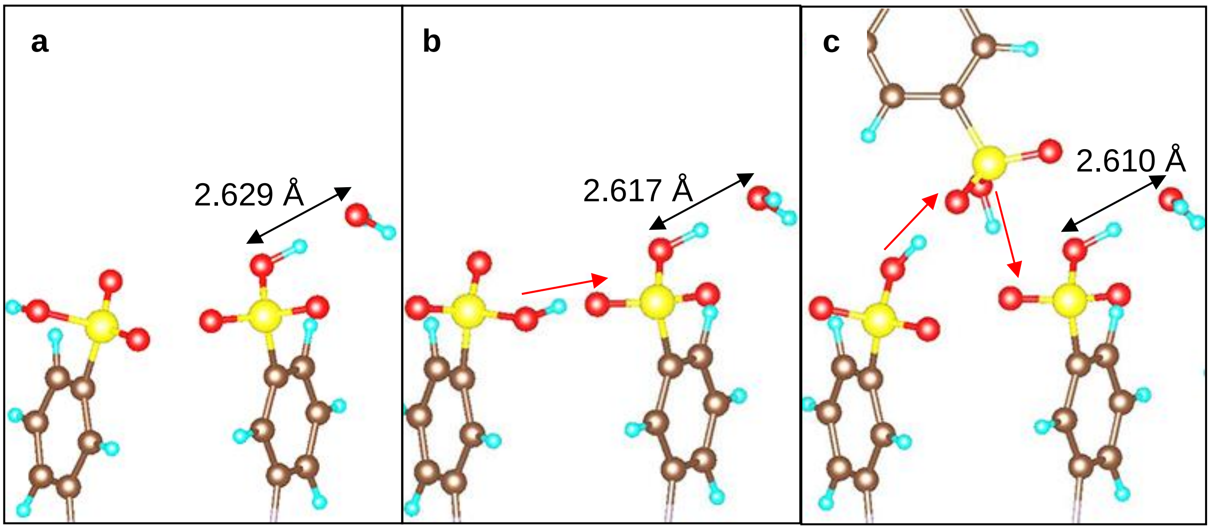

Figure S5.The effect of sequential sulfonic acids on *Roo*. (**a**) Water bound to sulfonic acid without sequential SO_3H. (**b**) Water bound to sulfonic acid with one sequential SO_3H. (**c**) Water bound to sulfonic acid with two sequential SO_3H molecules. The value of *Roo* between water and SO_3H is closely related to the number of sequential SO_3H molecules.

Although this strong contraction also causes pseudo-shuttling, the packed-acid mechanism can eliminate pseudo-shuttling. In our AIMD calculations, we observed hopping, which is facilitated by sequential H-bonding and the packed-acid mechanism. Sequential H-bonding of sulfonic acid (red arrow) strongly contracts the terminal *Roo* (black arrow) ($SO_3H \rightarrow H_2O$ (S1), Fig. S6a). This contraction facilitates hopping and also causes pseudo-shuttling along the black arrow. However, this strong H-bonding does not disrupt reorientation in the packed-acid mechanism. Once a red-circled (Fig. S6b) proton hops from SO_3H to SO_3^-, a blue-circled proton of H_3O^+ can hop to the next H_2O and eliminate proton pseudo-shuttling between H_3O^+ and SO_3^- (Fig. S6b,c). Thus, hopping is also facilitated in the packed-acid mechanism.

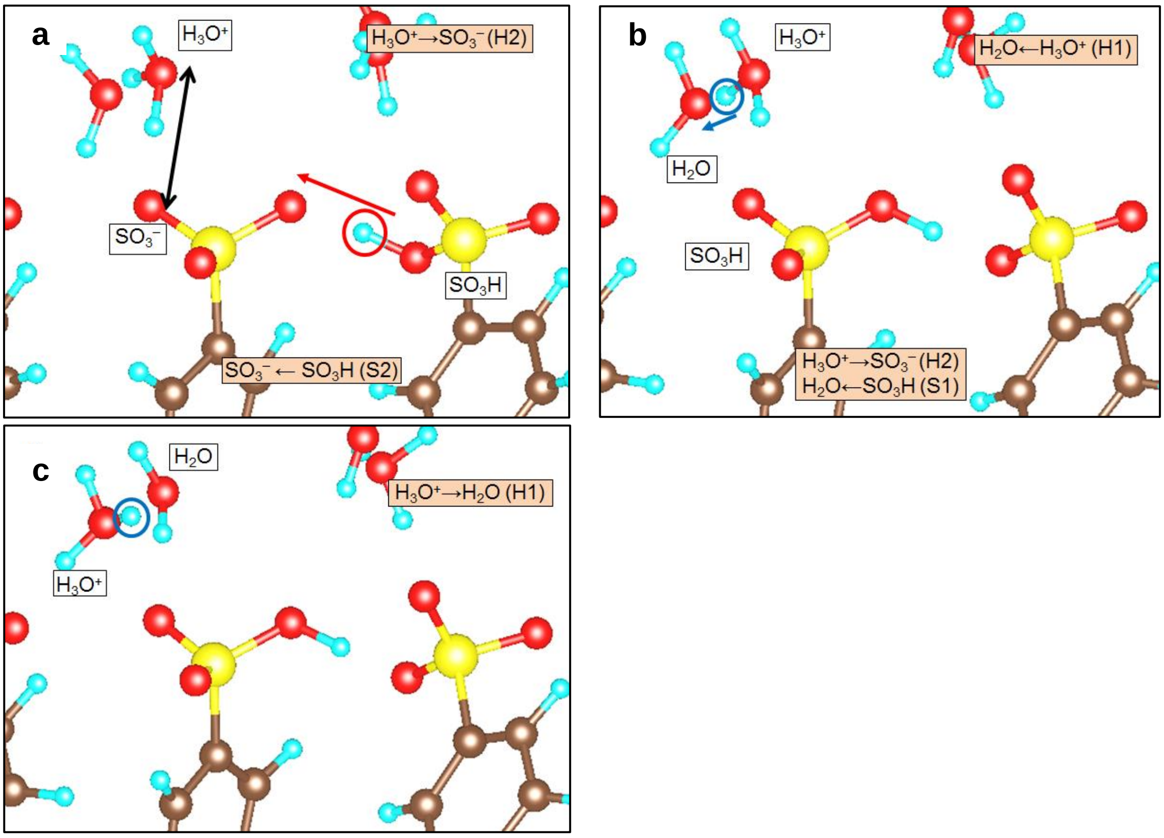

Figure S6. Another reorganization in the packed-acid mechanism.(**a**) The value of *Roo* along the black arrow increasingly contracts with the sequential H-bonding of sulfonic acid on the right (red arrow) to facilitate hopping. An acid can attract distant water molecules via H-bonding through sulfonic acid molecules and H^+. This attraction causes pseudo-shuttling between water and the SO_3^- on the left. (**b**) Once the SO_3^-on the left accepts a H^+ from the SO_3H on the right, pseudo-shuttling is eliminated in the packed-acid mechanism. (**c**) The blue-circled proton then hops to a water molecule.

VII. The origin of the high wavenumber of the asymmetric O–S–O stretching (O–S–O)

The general properties of the FT–IR spectra are discussed here, and we argue that the ZrSPP–BS model can describe the capping-ZrSPP–SPES interface. Table S3 describes the model at low λ; the packed acid structure has a high O–S–O wavenumber. The origin of this tendency was investigated using the model composed of BS and water molecules. Gaussian 09 was used for the model calculations with the B3LYP functional and 6-31G(d) basis set. The values of the wavenumbers obtained from these calculation methods were multiplied by 0.9613[S15]. In Table S4, S and W represent the BS and water molecules, respectively. The number of S and W indicates the number of BS and water molecules in each model; for example, model SWWW contains one BS and three water molecules. These models add BS or water molecules sequentially through an H-bond. Examples of the calculated models are shown in Fig. S7. The wavenumbers of O–S–O in each model, including BS (S) and BS without a proton (SO_3^-), are also listed in Table S4.

We can understand from the progression from SW to SWWW that the wavenumber energy of the O–S–O mode decreases when the number of water molecules bound to BS increases. A low wavenumber for O–S–O suggests that S–O bonding is weakened by the H-bond of water because the oxygen in S–O is attracted to the H-bond. The weakened bonding means that the energy of bond is decreased, leading to a low O–S–O wavenumber, *i.e.*, the H-bond generates a low O–S–O wavenumber.

By contrast, the wavenumbers of O–S–O in SSW, SSSW, and SSSSW suggest that there are two O–S–O wavenumber patterns: one in which BS binds to a water molecule (right BS in Fig. S7b) and has a low O–S–O wavenumber, and one in which BS does not bind to a water molecule (left and center BS in Fig. S7b) and has a high wavenumber. The first pattern possesses a low wavenumber because the binding energy between water and BS is high due to the indirect contraction shown in Fig. S5 (see section VI in SI). The strong H-bond causes a long S–O distance and low wavenumber. The second pattern has a high wavenumber due to its weak H-bonding, $SO_3H \rightarrow SO_3H$ (S3), $P_{<2.6} = 0$. The average O–S–O wavenumber in the model composed of many BS molecules approaches the simple BS model, which has a high O–S–O wavenumber because BS does not form a strong H-bond. By contrast, a model with only BS in the absence of a proton, SO_3^-, has a low O–S–O wavenumber.

As a summary of this section, the model with many water molecules allows BS to form many H-bonds and dissociate a proton to form SO_3^-, which results in a low O–S–O wavenumber. This model presumably works in the inactive region because of the isolated proton donor and low density of the acid groups, as shown in Fig. S4a. However, the model with concentrated BS has a high O–S–O wavenumber with a weak H-bond network composed of $SO_3H \rightarrow SO_3H$ (S3). This model describes the region activated by acid–acid interactions in Fig. S4b (see section V in SI). As shown in Fig. 5, the O–S–O of the capping-ZrSPP–SPES interface shifts to a higher wavenumber. The capping-ZrSPP–SPES interface subsequently has a packed-acid structure that can generate a weak H-bond network between sulfonic acid groups, $SO_3H \rightarrow SO_3H$ (S3). This interface structure with a weak H-bond network is generally difficult to generate because of the low bonding energy between the acids. However, the capping method can decide the morphology of the electrolyte before conversion from APS–Zr to ZrSPP. Therefore, sulfonic acids at the capping-ZrSPP–SPES interface might be required to form a weak H-bond network in the packed-acid structure.

Table S3. Statistical data for the calculated O–S–O wavenumber. The variable λ represents the number of water molecules within the model per sulfonic acid molecule.

λ	Average O–S–O wavenumber (cm^{-1})	O–S–O sample number	Standard error
0	1242	4	17.1
1-5	1157	25	48.4
9	1117	18	59.3

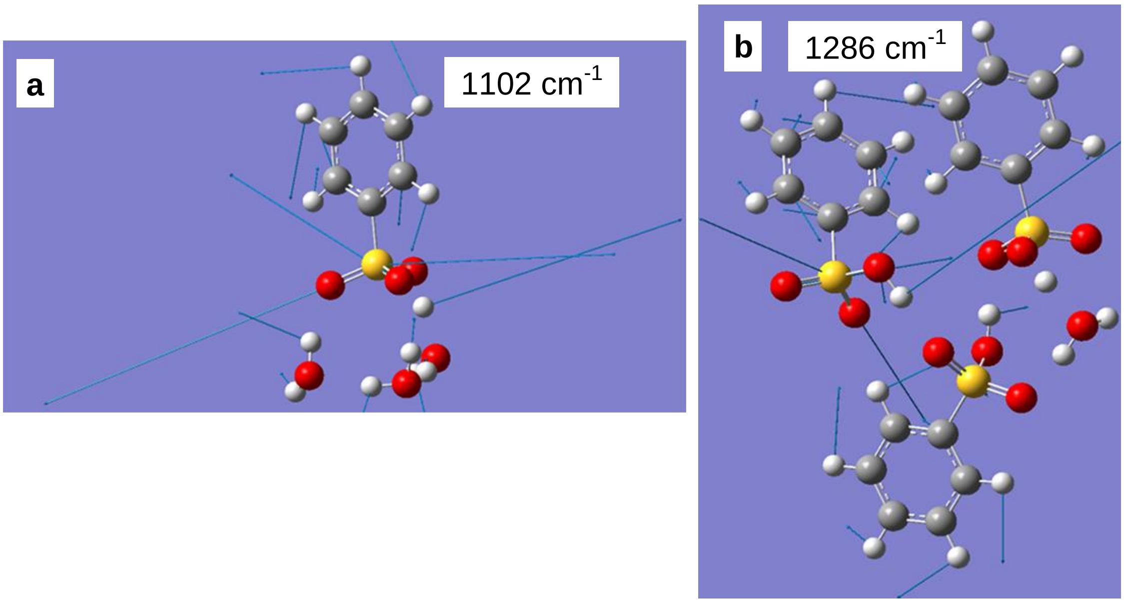

Figure S7. Examples of the O–S–O vibration in each model.(a) The SWWW model, which includes one BS and three water molecules. **(b)** The SSSW model, which includes three BS and one water molecule. The blue vectors indicate the direction and amplitude of the vibration.

Table S4. O–S–O wavenumbers in each model. These values have been multiplied by 0.9613[S15]. The highest O–S–O wavenumber is 1321 in S.

Range(cm^{-1})	$S(SO_3^-)$	· ·	SWWW	SWW	SW	SSW	SSSW	SSSSW	· ·	S
1100-1109			1102							
:										
1170-1179	1171, 1172									
1180-1189										
1190-1199								1199		
1200-1209							1203			
1210-1219			1216			1219	1213, 1215	1212, 1216		
1220-1229										
1230-1239				1238						
1240-1249						1247				
1250-1259					1252					
1260-1269						1261	1267			
1270-1279								1277		
1280-1289							1286			
1290-1299										
1300-1309								1303		1304
1310-1319								1319		
1320-1329										1321

VIII. Concerted hopping during AIMD

Concerted hopping was detected during AIMD with a typical occurrence depicted in Fig. S8. In Fig. S8a, a proton is involved in pseudo-shuttling in the direction of the black arrow between H_2O and SO_3^-. The protons in H-bonds along the red and blue arrows hop to the adjacent oxygen atom (Fig. S8b). These hopping events occur within 90 fs (fs = 10^{-15} s). The hopping in the direction of the red arrow occurs slightly before that in the direction of the blue arrow, with a time difference of only 30 fs. Thus, determining which hopping initiates the motion is difficult, although these hopping events also appear to be initiated by the same mechanism in Fig. S6 (see section VI in SI). Figure S8c indicates that hopping events in the direction of the pink arrow occur within 300 fs. Hopping on the 100-fs time scale is considered to occur in a concerted manner[S16–S18]. Thus, we conclude that these hopping events occur in a concerted manner.

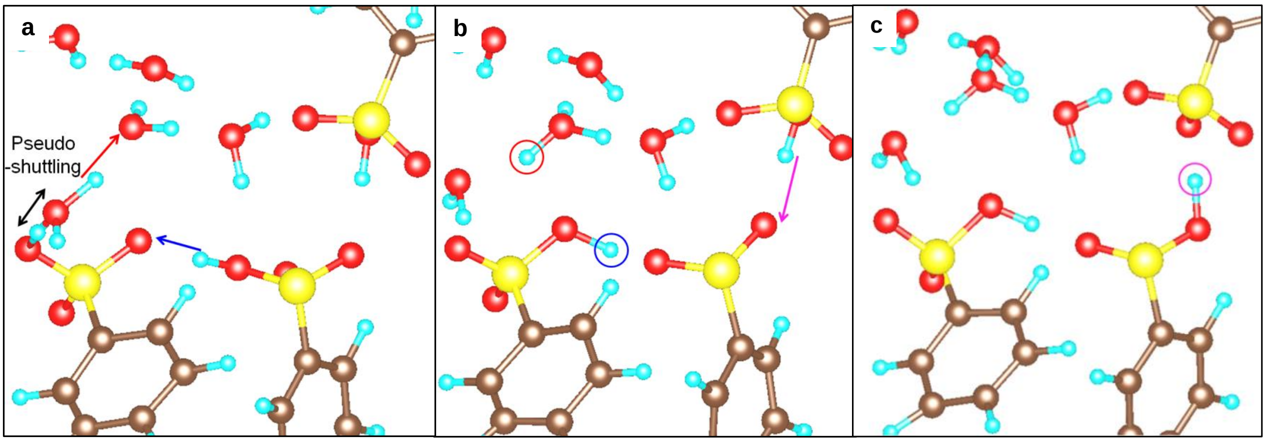

Figure S8. Concerted hopping (**a**) A proton is involved in pseudo-shuttling along the black arrow between H_2O and SO_3^-. (**b**) Protons in the H-bond along the red and blue arrows hop to the adjacent oxygen atom. (**c**) Hopping in the direction of the pink arrow occurs. The time differences between Figs. S8a and S8b and Figs. S8b and S8c are 90 and 300 fs, respectively. Thus, it can be concluded that these hopping events are concerted because the time differences are negligible[S16–S18].

IX. A suitable density of sulfonic acids (λ) for the packed-acid mechanism

A suitable density of sulfonic acids (λ) for the packed-acid mechanism is discussed. In Fig. S9, we focused on the H-bond from SO_3H or H_3O^+, with *Roo* classified as S1–3 or H1–3 in Fig. 9 and Table 1 because the H^+ directly involved in the interception of packed-acid mechanism is only in SO_3H or H_3O^+. We calculated the probability that *Roo* is shorter than 2.6 Å with *Roo* values classified as S1–3 or H1–3 ($P_{<2.6}$ *around* H^+) in each of the 42 structural patterns. $P_{<2.6}$ *around* H^+ is plotted against λ in Fig. S9. Figure S9 shows that the model with many water molecules has a high $P_{<2.6}$ *around* H^+, while the model with few water molecules has a low $P_{<2.6}$ *around* H^+.

In the model without water (λ = 0), only weak H-bonds exist ($P_{<2.6}$ *around* $H^+ = 0$ in Fig. S9), and the proton conduction is disrupted because of the infrequency of hopping. Thus, hopping and reorientation must occur equally for fast proton conduction. A $P_{<2.6}$ *around* H^+ of 50% appears to be suitable for the packed-acid mechanism, although the value of $P_{<2.6}$ *around* H^+ directly depends on the optimized structure in the models; a precise value is difficult to determine. According to Fig. S9, a $P_{<2.6}$ *around* H^+ of 50% is frequently obtained in the model with λ = 0.3-3 (the ratio of proton acceptors to donors), which seems to be a suitable density of sulfonic acids (λ) for the packed-acid mechanism.

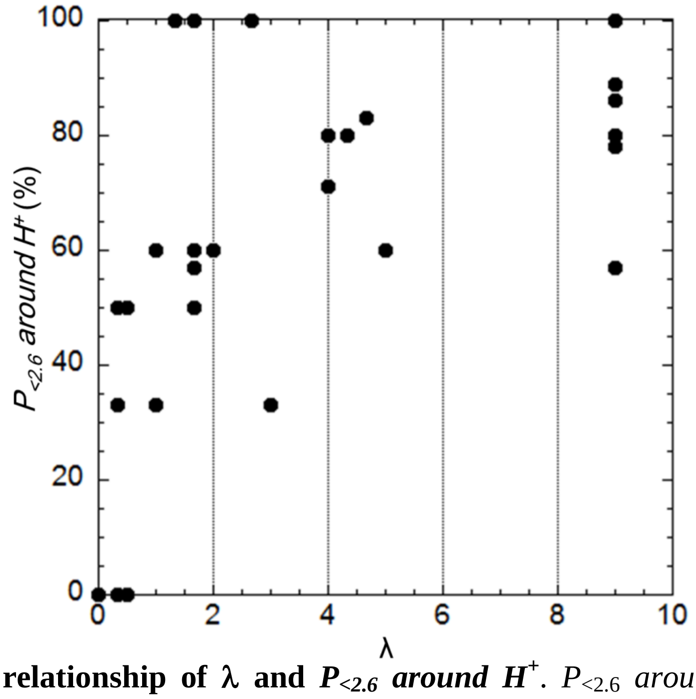

Figure S9. The relationship of λ and $P_{<2.6}$ *around* H^+. $P_{<2.6}$ *around* H^+ is plotted against λ. The model with many water molecules leads to a high $P_{<2.6}$ *around* H^+, while the model with few water molecules leads to a low $P_{<2.6}$ *around* H^+.

X. References

S1. Lee, J. M., Kikuchi, Y., Ohashi, H., Tamaki, T. & Yamaguchi, T., Novel mild conversion routes of surface-modified nano zirconium oxide precursor to layered proton conductors. *J. Mater. Chem.***20**, 6239-6244 (2010).

S2. Casciola, M. *et al.*, Nanocomposite membranes made of zirconium phosphate sulfophenylenphosphonate dispersed in polyvinylidene fluoride: Preparation and proton conductivity. *Solid State Ionics.***176**, 2985-2989 (2005).

S3. Alberti, G., Casciola, M., Pica, M., Tarpanelli, T. &Sganappa, M., New preparation methods for composite membranes for medium temperature fuel cells based on precursor solutions of insoluble inorganic compounds. *Fuel Cells.***5**, 366-374 (2005).

S4. Nakajima, T., Tamaki, T., Ohashi, H. & Yamaguchi, T., Introduction of size-controlled Nafion/ZrO_2 nanocomposite electrolyte into primary pores for high Pt utilization in PEFCs. *J. Electrochem. Soc.***160**, F129-F134 (2013).

S5. Wang, F., Hickner, M., Kim, Y. S., Zawodzinski, T. A. & McGrath, J. E., Direct polymerization of sulfonated poly(arylene ether sulfone) random (statistical) copolymers: candidates for new proton exchange membranes. *J Membrane Sci* **197**, 231-242 (2002)

S6. Alberti, G., Casciola, M., Palombari, R. &Peraio, A., Protonic conductivity of layerd zirconium phosphonates containing -SO_3H groups. II Ac conductivity of zirconium alkyl-sulphophenyl phosphonates in the range 100-200 °C, in the presence or absence of water vapour. *Solid State Ionics.***58**, 339-344 (1992).

S7. Lee, Y. J.; Bingol, B.; Murakhtina, T.; Sebastiani, D.; Meyer, W. H.; Wegner, G.; Spiess, H. W., High-Resolution Solid-State NMR Studies of Poly(vinyl phosphonic acid) Proton-Conducting Polymer: Molecular Structure and Proton Dynamics . *J. Phys. Chem. B* **2007**, *111*, 9711-9721.

S8. Kleinman, L. & Bylander, D. M., Efficacious form for model pseudopotentials. *Phys. Rev. Lett.***48,** 1425-1428 (1982).

S9. Troullier, N. & Martins, J. L., Efficient pseudopotentials for plane-wave calculations. *Phys. Rev. B.***43,** 1993-2006 (1991).

S10. Troup, J. M. & Clearfield, A., On the mechanism of ion exchange in zirconium phosphates. 20. refinement of the crystal structure of α-zirconium phosphate. *Inorg. Chem.***16**, 3311-3314 (1977).

S11. Momma, K. & Izumi, F., VESTA: a three-dimensional visualization system for electronic and structural analysis. *J. Appl. Crystallogr.***41**, 653-658 (2008).

S12. Arunan, E. *et al.*, Definition of the hydrogen bond (IUPAC Recommendations 2011). *Pure Appl. Chem.***83**, 1637-1641 (2011).

S13. Narten, A. H., Danford, M. D. & Levy, H. A., X-ray diffraction study of liquid water in the temperature range 4-200 °C. *Discuss. Faraday Soc.***43**, 97-107 (1967).

S14. Ogawa, T., Ushiyama, H., Lee, J. M., Yamaguchi, T. & Yamashita, K., Theoretical studies on proton transfer among a high density of acid groups: Surface of zirconium phosphate with adsorbed water molecules.*J. Phys. Chem. C.***115**, 5599-5606 (2011).

S15 Foresman,J. B., Frisch, A., *Exploring Chemistry With Electronic Structure Methods: A Guide to Using Gaussian.* (Gaussian Inc, Wallingford, 1996).

S16. Cox, M. J., Timmer, R. L. A., Bakker, H. J., Park, S. &Agmon, N., Distance-Dependent Proton Transfer along Water Wires Connecting Acid-Base Pairs. *J. Phys. Chem. A***113**, 6599-6606 (2009).

S17. Brewer, M. L., Schmitt, U. W. & Voth, G. A., The formation and dynamics of proton wires in channel environments. *Biophys. J.***80**, 1691-1702 (2001).

S18. Cui, Q. &Karplus, M., Is a "proton wire" concerted or stepwise? A model study of proton transfer in carbonic anhydrase. *J. Phys. Chem. B***107**, 1071-1078 (2003).

S19. Lee, Y. J.; Bingol, B.; Murakhtina, T.; Sebastiani, D.; Meyer, W. H.; Wegner, G.; Spiess, H. W. High-Resolution Solid-State NMR Studies of Poly(vinyl phosphonic acid) Proton-Conducting Polymer: Molecular Structure and Proton Dynamics. *J. Phys. Chem. B* ***111***, 9711-9721 (2007).